ACS Catalysis

Research Article

pubs.acs.org/acscatalysis

Analysis of Kinetics and Reaction Pathways in the Aqueous-Phase Hydrogenation of Levulinic Acid To Form γ-Valerolactone over Ru/C

Omar Ali Abdelrahman,[†] Andreas Heyden,[‡] and Jesse Q. Bond[†,*]

[†]Department of Biomedical and Chemical Engineering, Syracuse University, Syracuse, New York 13244, United States

[‡]Department of Chemical Engineering, University of South Carolina, Columbia, South Carolina 29208, United States

Supporting Information

ABSTRACT: Reaction pathways and kinetics governing the Ru-catalyzed hydrogenation of levulinic acid (LA) in the aqueous phase to form γ-valerolactone (GVL) were considered in a packed bed reactor. GVL can be produced by two distinct hydrogenation pathways; however, over Ru/C at temperatures below 423 K, it forms exclusively via intramolecular esterification of 4-hydroxypentanoic acid (HPA). Over Ru/C, reasonable hydrogenation rates of LA to HPA were observed at near-ambient temperatures (e.g., 0.08 s^{-1} at 323 K), but GVL selectivities are poor (<5%) under these conditions. Apparent barriers for LA hydrogenation and HPA esterification are 48 and 70 kJ mol^{-1}, respectively, and GVL selectivity improves at higher temperatures alongside increasing mass transfer limitations in 45−90 μm catalyst particles. Reactivity and selectivity trends in LA hydrogenation below 343 K are well-described by an empirical kinetic model capturing sequential hydrogenation and esterification. Coupling stacked beds of Ru/C and Amberlyst-15 delivers high GVL yields (~80%) at near ambient temperatures (323 K) and practical residence times.

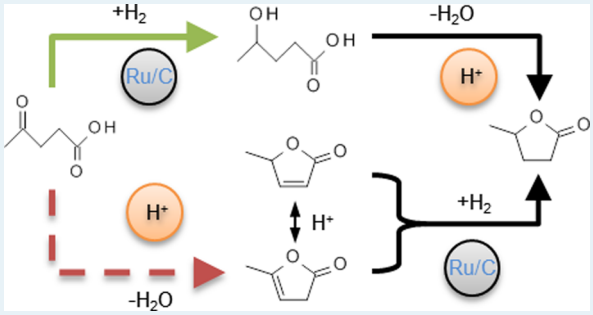

KEYWORDS: *levulinic acid, ruthenium, γ-valerolactone, hydroxypentanoic acid, angelicalactone, aqueous phase kinetics, hydrogenation*

1. INTRODUCTION

γ-Valerolactone (GVL) is of interest as a lignocellulosic platform chemical that offers tremendous flexibility in downstream applications and upgrading. For example, GVL can serve directly as a gasoline blender[1] or be subsequently processed to yield relatively energy-dense fuel additives, such as methyltetrahydrofuran,[2] valeric biodiesel,[3] or liquid alkanes.[4−10] GVL is also remarkably versatile as a biorefining solvent,[11] particularly for expediting the production of sugars, furans, levulinic acid (LA), and their numerous derivatives from lignocellulose.[12−17] Finally, GVL can be converted to chemical intermediates such as 1,4 pentanediol,[2] alkyl pentenoates,[18] and α-methylene-γ-valerolactone,[19] any of which may find application in the production of biobased polymers. The primary route envisioned for the production of lignocellulosic GVL is hydrogenation of levulinic acid,[20] which may be prepared from both 5- and 6-carbon sugars present in cellulose and hemicellulose through hydrolysis of either 5-hydroxymethylfurfural or furfuryl alcohol.[21−30] There are multiple options for selective hydrogenation of LA, and both homogeneous[2] and heterogeneous systems[20] have been employed. Despite burgeoning interest in transfer hydrogenation for GVL production,[31−33] the majority of LA hydrogenation processes have used molecular H_2 as a reducing agent and supported metals, such as Cu,[34,35] Ru,[19,36−39] Ir,[40] Au,[33] or bimetallics, such as RuRe[41,42] or RuSn[43,44] as catalysts. Further, recent studies focusing on the scale-up and economic feasibility of a GVL-centered biorefinery have favored Ru or Ru-bimetallics, which offer good hydrogenation rates, high GVL selectivity, and (particularly in the case of bimetallics) good stability.[7,41,42,45] Thus, detailed consideration of the kinetics of LA hydrogenation over Ru is warranted.

Between temperatures of 298 and 473 K and over supported Ru catalysts, LA is converted selectively to GVL via reduction with molecular H_2 (10−35 bar).[7,46] Producing GVL requires both hydrogenation and dehydration of LA, and we may envision two different pathways for the transformation, depending on the order in which dehydration and hydrogenation occur (Scheme 1).

Pathway 1 illustrates the sequence initiated by hydrogenation of the ketone group in LA to form 4-hydroxypentanoic acid (HPA). Subsequently, HPA undergoes acid-catalyzed, intramolecular esterification (ring closure) to form the thermodynamically preferred lactone, GVL. Alternatively, angelicalactones (AL) can form via endothermic dehydration of LA, and they become increasingly prevalent in acidic media and at elevated temperatures (pathway 2). In the presence of Ru/C and under H_2 atmospheres, angelicalactones are anticipated to rapidly hydrogenate, forming GVL. To date, the relative contributions of each pathway have not been delineated, and it is unclear which reactions in the above network are kinetically significant. Further, depending on operating conditions,[20,47]

Received: December 10, 2013
Revised: February 14, 2014
Published: February 28, 2014

   dx.doi.org/10.1021/cs401177p | ACS Catal. 2014, 4, 1171−1181

Scheme 1. Pathways Leading to γ-Valerolactone during Hydrogenation of Levulinic Acid

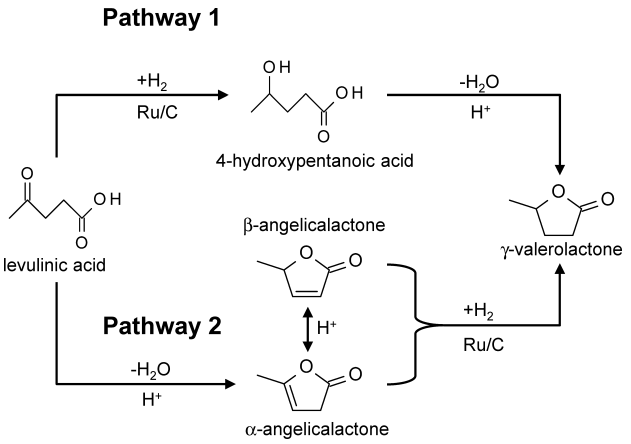

choice of solvent,[46,48−50] presence of metal promoters (e.g., Re or Sn),[42,44] and presence of residual impurities in levulinic acid feeds (e.g., H_2SO_4 or acid-soluble lignin),[42] Ru-based catalysts can display pronounced differences in both hydrogenation activity[20,36] and on-stream stability.[42]

Here, we present an investigation of the reaction pathways and kinetics of aqueous-phase LA hydrogenation over supported Ru, which is representative of LA feedstocks obtained via acid hydrolysis of lignocellulose. Kinetic studies have been carried out only for monometallic Ru/C having a single metal loading (5 wt %). Our motivation in doing so is to establish governing phenomena on a practically employed catalyst in the absence of confounding effects, thus providing a foundation for subsequent studies examining the influence of Ru promoters and feed impurities in greater detail. In consideration of this model system, we have decoupled HPA- and angelicalactone-mediated hydrogenation pathways to illustrate that GVL formation occurs primarily through ketone hydrogenation, followed by intramolecular esterification (pathway 1, Scheme 1). Upon identifying acid catalyzed intramolecular esterification of HPA as the kinetic bottleneck in GVL formation at low temperatures, we demonstrate that high yields of GVL can be achieved at 323 K using stacked beds of Ru/C followed by Amberlyst 15 (A15).

2. MATERIALS AND METHODS

Ru/C (5 wt %) was purchased from Strem Chemicals, and its surface area and average pore diameter were determined to be 756 m^2/g and 5.04 nm via N_2 adsorption at 77 K. Ru dispersion was calculated to be 40.4% from irreversible CO uptake at 308 K, assuming 1:1 adsorption stoichiometry. For 5 wt % Ru/C, this corresponds to a Ru site density of 200 $\mu mol\ g^{-1}$. Both N_2 and CO adsorption were performed using volumetric dosing in a commercial system (Micromeritics ASAP 2020). Before N_2 dosing experiments, samples were heated under vacuum (6 h, 623 K) to remove physisorbed impurities. Samples were prepared for CO chemisorption by reducing in flowing H_2 (3 h, 623 K, 3 K min^{-1}), evacuating at 623 K (1 h) to remove chemisorbed hydrogen, and cooling to 308 K under vacuum. Analysis was performed by collecting a CO adsorption isotherm at 308 K, evacuating the sample at 308 K (1 h) to remove physisorbed CO, and collecting a second isotherm at 308 K. Irreversible uptake was determined as the difference in CO uptake between the two isotherms.

Levulinic acid (LA, 98%, Sigma Aldrich), γ-valerolactone (GVL, 98%, Sigma Aldrich), sulfuric acid (95−98 wt %, Sigma Aldrich), and acetonitrile (HPLC grade 99.9% purity, Fisher Scientific) were employed as supplied by the manufacturer. A 4-hydroxypentanoic acid (HPA) calibration standard was synthesized by alkaline hydrolysis of GVL in sodium hydroxide (1 M) to produce 4-hydroxypentanoate, which forms HPA upon protonation. HPA used in esterification kinetic studies was synthesized via partial hydrogenation of aqueous LA (0.5 M) over Ru/C in a packed bed reactor (298 K, 23 bar H_2). After synthesis, esterification feeds were refrigerated (275 K) to minimize ring closure during storage (<24 h), but some amount of GVL formation was inevitable. Zero-time concentrations of HPA, LA, and GVL were thus rigorously determined by HPLC analysis (see online Supporting Information) prior to starting each experiment. Concentrations of HPA (0.04−0.06 M), LA (0.15−0.45 M), and GVL (5×10^{-4} to 1.5×10^{-3} M) varied depending upon the intended experiment. Water used in preparing reactor feeds, calibration standards, and HPLC mobile phases was purified in house by sequential reverse osmosis, UV oxidation, and double ion exchange. H_2 (99.999%, Airgas), N_2 (99.999%, Airgas), CO (99.99% Praxair) employed in flow systems and chemisorption experiments were used without further purification.

2.1. Kinetic Studies. Kinetic data were collected for three separate reactions illustrated in Scheme 1. First, the rate of LA hydrogenation over Ru/C was determined in a packed bed reactor under a H_2 atmosphere. Second, LA dehydration rates were quantified under typical LA hydrogenation conditions over Ru/C in a packed bed reactor under a nonreducing atmosphere. Finally, HPA esterification to form GVL was carried out in a batch reactor. Details for each experiment are provided in the following subsections.

2.1.1. Levulinic Acid Hydrogenation. Prior to use in kinetic studies, 5 wt % Ru/C was graded through a series of standard mesh sieves. Unless otherwise noted, particles in the range of 45−90 μm were used. Before loading into reactors, the stock catalyst was diluted to 1 g 5 wt % Ru/C per 99 g 45−90 μm quartz particles, which were obtained by milling and grading fused quartz granules (4−20 mesh SiO_2, Sigma Aldrich). One to five milligrams of undiluted 5 wt % Ru/C was generally required for typical reactor operation; as such, we employed a high dilution ratio to improve precision in catalyst mass loading. Reference experiments confirmed that hydrogenation rates were independent of the dilution scheme, suggesting that this protocol does not induce bypassing of the catalyst particles.

Hydrogenation of LA was carried out using the above-described Ru/C dilution in a concurrently fed, stainless steel packed bed reactor (1/4 in. × 12 in.). The reactor was operated in an upflow configuration over a range of temperatures (323−423 K) and H_2 pressures (4.1−41.5 bar). Relatively small amounts of catalyst were required for all of the studies reported here, and bed lengths were on the order of 0.5−1.0 in. Catalyst beds were positioned at the center of the heated section of the reactor and held in place by two quartz wool plugs. The tube upstream of the catalyst bed was packed with coarse (850−1200 μm) quartz granules to minimize dead volume, and the section immediately downstream of the catalyst bed was packed with smaller quartz granules (<45 μm) to minimize entrainment of carbon fines. Quartz packing was fixed in place with two quartz wool end plugs, and the reactor was placed in line using compression fittings.

dx.doi.org/10.1021/cs401177p | ACS Catal. 2014, 4, 1171−1181

Aqueous LA feeds (0.025−1.5 M) were introduced to the system using an HPLC pump (Lab Alliance Series 1). H_2 feeds were regulated by mass flow controller (Brooks 5850S) and mixed with the aqueous feed prior to introduction into the reactor. To ensure thermal equilibration of the reactor feed, both the H_2 and the aqueous LA feeds were circulated through a preheater section that was maintained at reactor temperature. Feed temperature was monitored by an in-line type K thermocouple and controlled using a PID controller (Love 16A-3010). The combined feed was then introduced to the packed bed, which was positioned in the center of a 2 in. aluminum rod held within a ceramic furnace (Applied Test Systems). Reactor temperature was monitored at the external wall of the catalyst bed using a type K thermocouple and controlled with a PID controller. System pressure was controlled using a back-pressure regulator (Tescom model 26-1766-24) and monitored both upstream and downstream of the packed bed using analog pressure gauges. The effluent of the system flowed directly into a vapor−liquid separator. Because no volatile products are formed during this reaction, the gas phase was vented continuously without analysis. The aqueous product was collected at regular intervals (15−30 min) and analyzed immediately using HPLC (Agilent 1100 Series). Full details of the analytical protocols are given in the Supporting Information. Prior to use, catalyst beds were reduced in situ (673 K, 4 h hold, 1 K min^{-1}) under flowing H_2 (100 SCCM, 1 bar).

Since LA hydrogenation occurs in a three-phase system, we anticipate that interphase, interparticle, and intraparticle transport limitations may govern concentrations of LA, dissolved H_2, and temperature at catalytic centers and thus control the rate of hydrogenation. A thorough consideration of transport and kinetically controlled operating regimes, along with the calculation of dissolved H_2 concentrations, is presented in the Supporting Information. For the experiments described here, we observed that interphase H_2 transport is rapid such that dissolved H_2 concentrations are well-approximated by their equilibrium value, as determined by gas-phase H_2 pressures and Henry's law. Further, linear fluid velocities at or beyond volumetric aqueous feed rates of 0.4 mL min^{-1} are sufficiently high to eliminate any external concentration or temperature gradients. Finally, for 5 wt % Ru/C, intraparticle transport limitations were negligible at and below 343 K for catalyst particles smaller than 125 μm.

Where higher conversions are not otherwise indicated, reactors operated differentially (<3% LA conversion), and the only reaction products observed were HPA and GVL. Because conversion ranges for differential operation are within the precision expected of mass balance closure and HPLC analysis, LA conversion and product selectivity were determined on the basis of product formation as defined in eqs 1 and 2, where n_{HPA} and n_{GVL} are the total molar quantities of HPA and GVL recovered in a given reactor sample, and n_{LA0} is the total molar quantity of LA fed into the system. Yield is calculated as the product of LA conversion, X_{LA}, and selectivity, S_i.

$$X_{LA} = \frac{n_{4HPA} + n_{GVL}}{n_{LA_0}} \quad (1)$$

$$S_i = \frac{n_i}{n_{HPA} + n_{GVL}} \quad (2)$$

Site time yields (STY) are reported for both HPA and GVL over a range of conversions. They were calculated according to eq 3.

$$STY_i = \frac{F_i}{m_{cat} \cdot \varphi_{Ru}} \quad (3)$$

where F_i is the effluent molar flow rate of either HPA or GVL, m_{cat} is the mass of catalyst in the bed, and φ_{Ru} is the loading of Ru surface sites per gram of catalyst as determined by CO chemisorption. In all data summarized here, site time yields have units of moles product per mole of Ru surface sites per second, which is reported as s^{-1} for convenience.

2.1.2. LA Dehydration. To probe the extent to which angelicalactones contribute to GVL formation, the baseline rate of LA dehydration was determined in an inert atmosphere over Ru/C. This experiment was motivated by the fact that C═C bond hydrogenation is anticipated to be rapid over Ru/C relative to LA dehydration, making it difficult to distinguish between GVL formed via LA dehydration and LA hydrogenation in a reducing environment. To provide an accurate accounting of GVL fractions formed by pathways 1 and 2 (Scheme 1), it is thus necessary to quantify the rate of dehydration independent of hydrogenation. To this end, a reference experiment was carried out identically to the protocol described in section 2.1.1 (LA Hydrogenation), with the exception that the H_2 feed was replaced with N_2 to suppress both LA and angelicalactone hydrogenation. Liquid phase products were analyzed by HPLC and gas chromatography, as described in the Supporting Information.

2.1.3. Intramolecular Esterification of HPA. The intramolecular esterification (ring closure) of 4-hydroxypentanoic acid (HPA) to form GVL was studied in batch reactors in dilute aqueous solutions of LA. A feed HPA solution was prepared by partial hydrogenation of LA, stored at 275 K to inhibit ring closure, divided into aliquots, and loaded into magnetically stirred autoclave reactors (10 mL) that were subsequently placed in a temperature-controlled oil bath. Batch experiments were conducted at ambient pressure and temperatures ranging from 300 to 339 K. To determine whether ring closure is heterogeneously catalyzed in this system, identical experiments were carried out with the addition of both Ru/C and quartz granules (0.05 g/g feed). Batch vessels were stirred at 700 rpm to eliminate extraparticle gradients, and solid particles of 45−90 um were employed to minimize internal diffusion limitations where relevant. LA, HPA, and GVL concentrations were monitored as a function of time by withdrawing 200 μL aliquots from the reactor using a syringe. Each sample was analyzed by HPLC as described in the Supporting Information. Intramolecular esterification of HPA was the only reaction observed in these experiments, and LA concentrations remained constant throughout. Solution pH was measured at ambient temperature at the beginning and end of every experiment, and we observed a maximum change of 2.3% in dissolved H^+ concentration over the course of a single experiment, indicating that HPA consumption did not have a significant effect on H^+ concentration. On the basis of previously compiled data regarding the effect of temperature on the dissociation of LA[51] and related carboxylic acids,[51−53] dissolved H^+ concentrations were determined to vary minimally (<5%) over the experimental temperature range (300−339 K). This observation is consistent with prior results,[54] and we

dx.doi.org/10.1021/cs401177p | ACS Catal. 2014, 4, 1171−1181

Table 1. Experimentally Observed LA Conversions and Product Selectivities during Hydrogenation of LA over Ru/C under Inert and Reducing Environments and at Temperatures Ranging from 323 to 423 K

					STY (s^{-1})			selectivity (%)		
run	gas	T (K)	WHSV (hr^{-1})	X_{LA} (%)	HPA	GVL	AL	HPA	GVL	AL
1	H_2	323	550	1	0.09	0.004		96	4	0
2	H_2	323	37	20	0.09	0.002		98	2	0
3	H_2	323	5.0	99	0.06	0.003		95	5	0
4	N_2	323	550	trace			5×10^{-7}	0	0	100
5	N_2	423	550	trace			1×10^{-6}	0	0	100
6	H_2	343	730	2	0.17	0.02		89	11	0
7	H_2	363	720	3	0.18	0.04		81	19	0
8	H_2	383	920	3	0.23	0.13		63	36	0
9	H_2	403	790	5	0.25	0.17		59	40	0
10	H_2	423	1500	3	0.12	0.48		19	81	0

therefore consider the measured starting pH to be constant throughout each experiment.

2.2. Stacked Bed Experiments. Ru/C and Amberlyst-15 were coupled in stacked beds to facilitate both LA hydrogenation and HPA ring closure in a single reactor at low temperatures. To accommodate the relatively low thermal stability of A15, Ru/C used in stacked beds was reduced ex situ in H_2 at 673 K and subsequently passivated at 298 K in 1% O_2/N_2. Passivated Ru/C and unmodified A15 were sequentially loaded into a single 1/4 in. stainless steel tube to create two stacked beds separated by a quartz wool plug. The entire bed was then reduced at 373 K (3 K min^{-1}) in 100 sccm of H_2 for 2 h to remove the oxygen monolayer from Ru surface sites. Control experiments confirmed that Ru/C reduced and passivated ex situ (used in stacked beds) performed identically to Ru/C reduced in situ (used in LA hydrogenation kinetic studies). As such, this experiment reveals only the effect of adding secondary acid functionality downstream of the hydrogenation system.

3. RESULTS AND DISCUSSION

3.1. Primary Analysis of LA Hydrogenation Products Formed over Ru/C. Table 1 summarizes experimental observations during the aqueous-phase hydrogenation of LA over Ru/C.

From data in entries 1−3, we observe that hydrogenation of LA over Ru/C at near ambient temperatures (323 K) yields only two products, HPA and GVL, over LA conversions ranging from 1 to 100%. Over the entire conversion range, we note that GVL selectivity is poor (<5%) at 323 K, and the major LA hydrogenation product is HPA (>95% selectivity). This suggests that the HPA-mediated pathway illustrated in Scheme 1 likely dominates GVL production and may indicate that intramolecular esterification of HPA, rather than hydrogenation of LA, controls the rate of GVL formation over Ru/C.

To further probe the extent to which angelicalactone formation contributes to GVL production, we consider entry 4, which is identical to entry 1 except that the reducing gas (H_2) has been replaced with an inert (N_2). Under these conditions, we observe trace LA conversion with complete selectivity to angelicalactones, indicating that in the absence of H_2, LA is consumed only by dehydration. However, the site time yield to angelicalactones over Ru/C (5×10^{-7} s^{-1}) is several orders of magnitude lower than site time yields observed for HPA (0.085 s^{-1}) and GVL (0.005 s^{-1}) in the presence of hydrogen (entry 1). Even upon increasing the system temperature to 423 K (entry 5), site time yields for dehydration (10^{-6} s^{-1}) remain well below hydrogenation rates summarized in entries 1−3. Since LA dehydration is essentially not observed over Ru/C relative to the scale of HPA and GVL production over the range of temperatures considered here (303−423 K), we conclude that GVL formation over Ru/C occurs exclusively through the HPA-mediated pathway (pathway 1, Scheme 1) in this temperature range.

Entries 6−10 compare HPA and GVL selectivity and site time yields at reaction temperatures from 343 K to 423 K. As the reaction temperature increases, LA hydrogenation rates increase, and GVL selectivity improves relative to HPA. This is attributed to an increase in the rate of ring closure relative to the rate of hydrogenation. Intramolecular esterification of HPA is reversible such that HPA/GVL distributions in hydrogenation products will ultimately be determined by chemical equilibrium. A concentration-based equilibrium constant for esterification of HPA in aqueous solution at 298 K was experimentally determined here to be 14.5, which is in good agreement with the mean value of those previously reported for this reaction (13.8).[55] HPA ring closure is estimated to be only slightly exothermic (−3 kJ/mol), on the basis of prior accounts of γ-hydroxybutyric acid esterification;[56] thus, equilibrium GVL selectivities are not expected to change drastically with increasing temperature and should exceed 90% at each experimental condition described here. This was confirmed by experimental observation, where nearly complete GVL selectivity was observed at chemical equilibrium over a range of temperatures from 298 to 423 K. We therefore conclude that HPA ring closure is not equilibrated in any of the experiments described in Table 1 and attribute the improved GVL selectivity to an increased rate of HPA esterification relative to the rate of LA hydrogenation. This suggests that HPA ring closure proceeds with a higher activation barrier than LA hydrogenation and may also reflect increasing mass transfer limitations in LA hydrogenation at high temperatures (see the Supporting Information).

3.2. Kinetics of LA Hydrogenation. Because LA dehydration is demonstrated to have a negligible contribution to GVL production below 423 K (Section 3.1), the sum of production rates for GVL and HPA can be taken as the total rate at which the ketone group in LA is hydrogenated. Because differential conditions were maintained in kinetic studies reported hereafter, turnover frequencies for LA (ketone) hydrogenation are well-approximated as the sum of site time yields for HPA and GVL.

$$TOF_{LA} = STY_{HPA} + STY_{GVL} \quad (4)$$

dx.doi.org/10.1021/cs401177p | ACS Catal. 2014, 4, 1171−1181

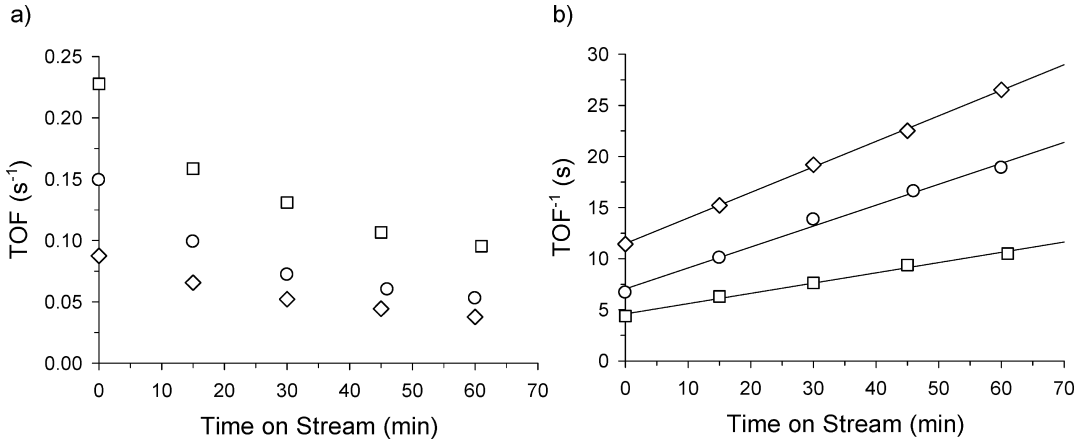

Figure 1. (a) Rates of LA hydrogenation over Ru/C at 323 K (◊), 343 K (○), and 363 K (□) as a function of time on-stream. (b) Linearized rate data illustrating second-order deactivation and method employed for estimation of rates at zero time on-stream. For all experiments summarized here, the aqueous phase concentrations of LA and H_2 were 0.50 and 0.016 M.

Figure 1 plots turnover frequencies of LA hydrogenation over Ru/C as a function of time on-stream at several representative reaction conditions. It is evident that LA hydrogenation rates decay rapidly in this aqueous-phase system, even at mild temperatures (323 K). Ultimately, we were unable to identify an operating regime in which deactivation does not occur; as such, initial turnover frequencies at a given experimental condition were estimated by extrapolation of rate data to zero time on-stream. Independent of the reaction conditions, the time decay of hydrogenation rates at short times on-stream (below 8 h) was well-described by a second-order model such that declining reaction rates can be linearized by plotting inverse turnover frequencies against time on-stream, as described by Bartholomew.[57] Regression of linearized data sets permits quantification of initial hydrogenation turnover frequencies via estimation of a *y*-intercept, and all initial turnover frequencies reported here for LA hydrogenation were approximated using this method.

Detailed consideration of Ru/C deactivation is outside the focus of this article; however, some discussion is warranted because of the ubiquity of noble metal-on-carbon catalysts in emerging aqueous phase hydrogenation processes targeting biorenewables. Figure 2 summarizes on-stream performance of Ru/C during LA hydrogenation at 323 K. Here, we observe that TOFs for LA hydrogenation ultimately stabilize at 20−30% of their original values after 48−72 h on stream. Regeneration attempts via in situ reduction reveal that this loss of activity occurs through a combination of reversible and irreversible phenomena. After reaching steady state, catalysts can be restored to only 50−60% of their initial activity, and their renewed activity decays quickly (within 5 h) to the steady state value after being placed on-stream again. To date, the mode of reversible deactivation has not been conclusively identified, but it may be attributed to either strongly bound hydrocarbon intermediates or surface oxidation of Ru nanoparticles.

With respect to irreversible deactivation, we have not observed Ru leaching or attrition of the carbon support in this system; neither does the carbon support undergo significant physical changes as determined by N_2 adsorption. As such, irreversible deactivation observed here is most likely attributed to particle sintering. Ru dispersion, determined by CO chemisorption, decreases from 40% to 21% in pre- and postreaction samples. Because leaching, attrition, and structural

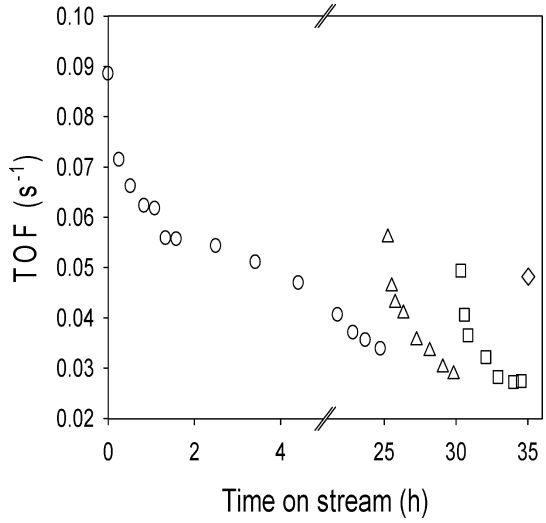

Figure 2. Observed LA hydrogenation rates as a function of time on-stream at T = 323 K, C_{H_2} = 0.016 M, C_{LA} = 0.1 M. (○) Fresh catalyst, (Δ) first regeneration, (□) second regeneration, (◊) third regeneration. Regeneration was performed in situ by interrupting aqueous feeds and reducing the catalyst under flowing H_2 (100 sccm, 4 h, 673 K, 1 K min^{-1}).

degradation have not been observed, this loss of dispersion suggests an increase in Ru cluster size from roughly 3.6 nm in fresh samples to 6.8 nm in samples recovered after 65 h on-stream. Sintering is typically considered a high temperature phenomenon; however, water can facilitate particle agglomeration close to room temperature.[58] These observations are supported by the works of Davis, who reported metal cluster growth during aqueous phase hydrogenation of glucose over Ru/SiO_2 at 373 K,[59] and Marin, who observed particle growth from 2.2 to 3.2 nm during the aqueous phase oxidation methyl-α-D-glucoside over Pt/C.[60] Sintering is thus a realistic consideration in this system, and future efforts geared toward rational design of stable hydrogenation catalysts for biomass processing should consider strategies for maintaining high Ru dispersions in the aqueous phase. In the interest of brevity and maintaining a focus on the kinetics of LA hydrogenation, we will defer a more comprehensive characterization of spent catalyst samples to subsequent communications. In the

dx.doi.org/10.1021/cs401177p | ACS Catal. 2014, 4, 1171−1181

remainder of this section, we discuss observed trends in initial LA hydrogenation turnover frequency as a function of LA concentration, dissolved H_2 concentration, and reaction temperature.

3.2.1. Reaction Orders. Levulinic Acid. The concentration of LA in the aqueous phase was found to have a minimal and slightly inhibitory effect on the initial rate of hydrogenation. This trend is illustrated in Figure 3, and regression of the data

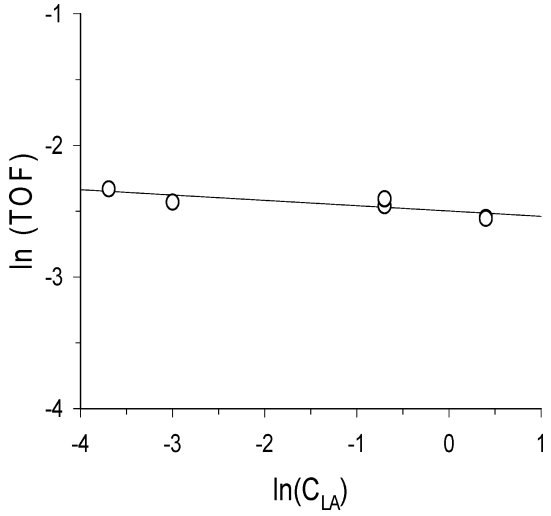

Figure 3. Correlation between levulinic acid concentration and hydrogenation rate. Experiments illustrated here were carried out at 323 K, 0.016 M H_2 concentration, and varying WHSV to maintain LA conversions below 3%. Turnover frequencies are reported in s^{-1}, and LA concentrations are reported in mol L^{-1}.

there reveals an apparent reaction order of -0.04 ± 0.04 over a range of LA concentrations (0.025−1.5 M), indicating that the rate of LA hydrogenation is nearly independent of bulk LA concentrations over practical values. This observation is consistent with prior studies of both gas and liquid phase reactions in which apparent zero-order kinetics with respect to the hydrocarbon are generally observed for both C═O and C═C hydrogenations over group VIII metals. For example, both hydrogenation of D-glucose[61] and arabinonic acid[62] are zero-order in the oxygenate over Ru/C above concentrations of 0.3 and 1 M, respectively. Other supported, noble metals exhibit similar behavior. For example, Vannice has reported that benzene[63] and citral[64] hydrogenation over supported Pt and Pd catalysts, respectively, are zero-order in organic concentration. Similarly, for the gas phase hydrogenation of ethylene over Pt, Dumesic observed zero-order dependence on ethylene at low temperatures and high partial pressures of ethylene.[65] Apparent zero-order dependencies on organic species during hydrogenation is typically attributed to the presence of strongly bound hydrocarbon intermediates that saturate available metal surface sites during hydrogenation.[66] A more detailed interpretation will be provided in section 3.2.3.

Hydrogen. Figure 4 illustrates the dependence of hydrogenation turnover frequency on the concentration of dissolved hydrogen in the aqueous phase. Here, a pronounced effect is observed, and regression of the rate data reveals a fractional order of 0.6 ±0.2. This outcome suggests that H_2 adsorption is rapid, such that surface reactions involving the addition of atomic hydrogen to adsorbed organic species control the rate of LA hydrogenation. Similar half-order hydrogen dependencies

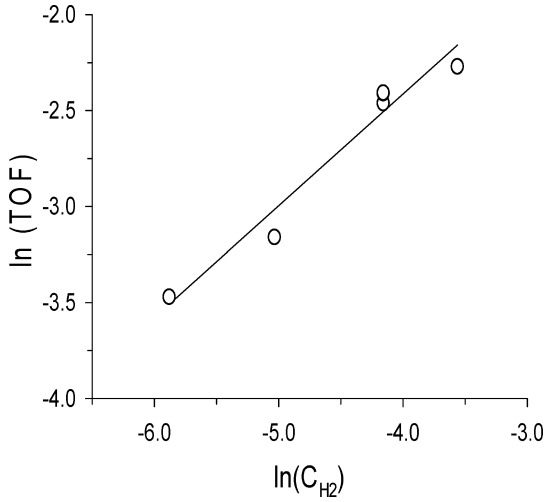

Figure 4. Correlation between dissolved aqueous phase hydrogen concentration and hydrogenation rate. Experiments illustrated here were carried out at 323 K, 0.5 M LA, and varying WHSV to maintain LA conversions below 3%. Turnover frequencies are reported in s^{-1}, and H_2 concentrations are reported in mol L^{-1}.

were observed by Vannice during benzene and acetic acid hydrogenation over supported Pt,[63,67] Dumesic during ethylene hydrogenation over Pt,[65] and Mahajani in the hydrogenation of *n*-valeraldehyde[68] and *iso*-valeraldehyde[69] over supported Ru. Reconciliation between this observation and a proposed reaction pathway will be discussed in subsequent analysis (section 3.2.3). At this stage, our consideration of apparent reaction orders suggests that LA hydrogenation is well-represented under the conditions reported here by the empirical rate law given in eq 5.

$$r_{LA} = k' \cdot c_{H_2}^{1/2} \quad (5)$$

3.2.2. Temperature Effects. Assuming the empirical rate law derived in the preceding section (eq 5) is valid over the range of experimental conditions tested, we can estimate apparent rate constants for the hydrogenation of LA by normalizing measured turnover frequencies by the square root of the concentration of dissolved hydrogen. Subsequently, we may examine their temperature dependence to extract apparent activation energies and pre-exponential factors for this reaction. Apparent rate constants are plotted on a logarithmic scale against inverse temperature in Figure 5, which reveals two distinct regimes. At relatively high temperatures (363−423 K), the data suggest an apparent activation barrier of 20 ± 6 kJ mol^{-1}, which is lower than that anticipated of kinetic rate control and likely indicates that internal pore diffusion dominates at higher temperatures. This observation is consistent with our preliminary analysis of the Weisz−Prater criteria (see Supporting Information), which suggests that pore diffusion becomes significant at temperatures around 363 K. At lower temperatures (303−343 K), regression of linearized rate data indicate an apparent activation energy of 48 ± 5 kJ mol^{-1} and an apparent pre-exponential factor of roughly 3.1×10^7 $L^{0.5}$ $mol^{-0.5}$ s^{-1} on a Ru site basis or 6.2×10^3 $(L \cdot mol)^{0.5}$ $(g \cdot s)^{-1}$ on a catalyst mass basis. Importantly, data in the low temperature region were demonstrated to be free of internal diffusion limitations through the observation of invariant hydrogenation turnover frequencies as a function of mean particle size at 343 K (see Supporting Information). In line with our observations,

dx.doi.org/10.1021/cs401177p | ACS Catal. 2014, 4, 1171−1181

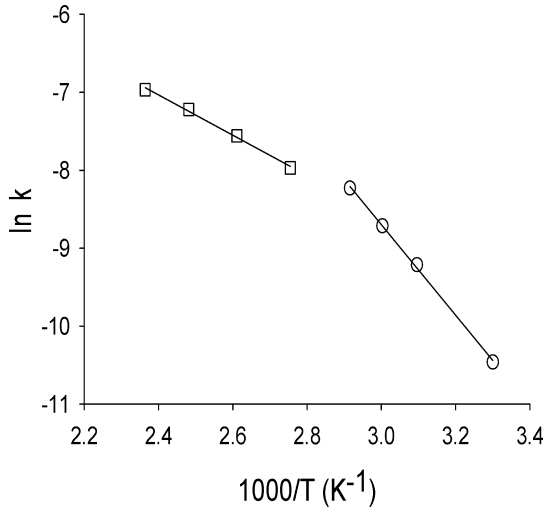

Figure 5. Correlation between reaction temperature and levulinic acid hydrogenation apparent rate constant. Experiments illustrated here were carried out at 0.5 M LA, 0.016 M H_2, and varying WHSV to maintain LA conversions below 3%. Apparent rate constants here are reported in $L^{0.5}$ $mol^{0.5}$ g^{-1} s^{-1}.

prior studies have reported activation barriers ranging from 34 to 64 kJ mol^{-1} over supported Ru for cinnamaldehyde,[70] D-lactose,[71] D-glucose,[61] and arabinonic acid.[62] Similar activation energies of hydrogenation were also reported over supported Pt for benzene[63] and ethylene.[65] We therefore consider that an apparent barrier on the order of 48 kJ mol^{-1} is reasonable for levulinic acid hydrogenation over Ru/C.

3.2.3. Analysis of Kinetic Data. The observed reaction orders and apparent activation energy align well with previously documented studies considering both C=O and C=C hydrogenation. All observations can be reconciled with a conventional Horiuti–Polanyi interpretation,[72] which is illustrated in a simplified scheme of LA hydrogenation in eqs 6–9. Briefly, according to this mechanism, LA adsorbs molecularly and H_2 adsorbs dissociatively at Ru surface sites. Surface-bound LA is subsequently reduced in two steps by sequential addition of hydrogen atoms, ultimately forming the hydroxyacid (HPA), which we assume desorbs irreversibly from the surface.

$$1.\ LA + * \leftrightarrow LA* \tag{6}$$

$$2.\ H_2 + 2* \leftrightarrow 2H* \tag{7}$$

$$3.\ LA* + H* \leftrightarrow LAH* + * \tag{8}$$

$$4.\ LAH* + H* \rightarrow HPA + 2* \tag{9}$$

On the basis of prior computational studies,[73] the half-hydrogenated intermediate (LAH, formed in step 3) is expected to be the dominant hydrocarbon species bound to Ru surface sites, and the second addition of atomic hydrogen (step 4) is generally considered to be rate-determining. This assumption will yield the overall rate expression for LA hydrogenation given by eq 10.

$$r = k_4 \cdot \theta_{LAH} \theta_H \tag{10}$$

Half-hydrogenated species are expected to adsorb favorably on Ru surface sites under most conditions.[66] If we make the assumption that H_2 adsorption and hydrocarbon adsorption are fully competitive and that the two species occupy identical surface sites, then we would expect (in the limit of a surface dominated by bound hydrocarbon intermediates) that the rate of hydrogenation would exhibit apparent reaction orders of −1 in LA and 0 in H_2, which are significantly different from our observed apparent orders of −0.04 and 0.6 for LA and H_2, respectively. Alternatively, our preliminary density functional theory results suggest that on flat terrace sites of Ru, adsorbed H-atoms are the dominant surface species. In this case, competitive adsorption of H_2 and hydrocarbon species would predict apparent reaction orders of +1 in LA and 0 in H_2, which is again significantly different from our observations. Data collected in the regimes summarized here are thus more easily reconciled with the assumption that surface-bound hydrocarbons and hydrogen atoms adsorb noncompetitively and can be considered in separate site balances. In the case of noncompetitive adsorption, we predict via Langmuir–Hinshelwood analysis that the overall hydrogenation rate should take the form given by eq 11.

$$r = \frac{k_4 K_1 K_2 K_3 C_{LA} C_{H_2}}{(1 + K_1 C_{LA} + K_1 K_2^{1/2} K_3 C_{LA} c_{H_2}^{1/2})(1 + K_2^{1/2} c_{H_2}^{1/2})} \tag{11}$$

Considering that the half-hydrogenated LAH intermediate is likely bound strongly and difficult to hydrogenate, we may apply the simplifying assumptions that the coverage of the hydrocarbon intermediate approaches saturation on sites available for hydrocarbon adsorption, and the coverage of levulinic acid approaches zero. The assumption of a small LA coverage is reasonable because close structural analogs, such as 2-butanone, are reported to bind weakly relative to hydrogenation intermediates at Ru sites.[73] Because we observe a distinct, positive reaction order with respect to hydrogen, we additionally assume that sites accessible to atomic hydrogen are far from saturation. Applying these limiting assumptions, the overall hydrogenation rate manifests as in eq 12, which reconciles well with our observed reaction orders of −0.04 and 0.6 in LA and H_2.

$$r = k_4 \cdot K_2^{1/2} c_{H_2}^{1/2} \tag{12}$$

3.3. Kinetics of the Intramolecular Esterification of HPA. As demonstrated in section 3.1, intramolecular esterification of HPA is the final step in the low-temperature production of GVL. Examination of selectivity trends suggests that HPA esterification is kinetically significant in the production of GVL over Ru/C, and we expect that this step is acid catalyzed. In the system considered here, the primary source of acidity is likely solvated protons dissociated from LA and HPA, both of which are weak organic acids having pK_a values of 4.59 and 5.69,[55] respectively. However, because oxidized carbon and Ru may also exhibit some acidity, we cannot conclude a priori that ring closure is exclusively a homogeneous reaction in this system. Prior to investigating reaction kinetics, control experiments were carried out to determine whether Ru/C and quartz influence the rate of HPA ring closure. At 303 K, we observed no difference in esterification rates observed with and without the addition of Ru/C and quartz, indicating that heterogeneous reactions do not contribute to HPA ring closure during hydrogenation. Subsequent sections describe experiments designed to capture reaction orders and temperature dependencies in the intramolecular esterification of HPA.

3.3.1. Reaction Orders. On the basis of the intramolecular esterification mechanism, we expect that the rate of ring closure

dx.doi.org/10.1021/cs401177p | ACS Catal. 2014, 4, 1171–1181

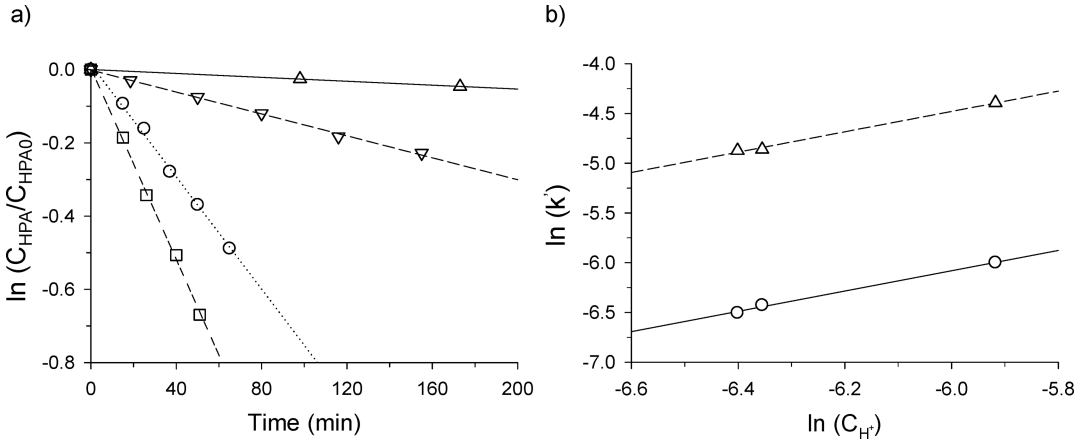

Figure 6. (a) Batch kinetic data for intramolecular esterification of HPA at (Δ) 300 K, C_{H^+} = 1.65 mM, C_{HPA_0} = 47.7 mM, (▽) 318 K, C_{H^+} = 1.65 mM, C_{HPA_0} = 47.7 mM, (○) 339 K, C_{H^+} = 1.65 mM, C_{HPA_0} = 47.7 mM, (□) 339 K, C_{H^+} = 2.69 mM, C_{HPA_0} = 41.2 mM. (b) Apparent rate constants for intramolecular esterification of HPA determined at (Δ) 339 and (○) 318 K at various pH values. k' is reported here in units of min^{-1}.

will exhibit some dependence on the concentrations of HPA and dissolved protons, as summarized in eqs 13 and 14.

$$r = k' \cdot C_{HPA}{}^{\alpha} \tag{13}$$

$$k' = k \cdot C_{H^+}{}^{\beta} \tag{14}$$

For a set of batch kinetic studies having varied HPA concentrations, LA concentrations, and reaction temperatures, Figure 6a illustrates HPA concentration normalized by its initial value as a function of time on a logarithmic scale. The demonstration of linearity in each data set indicates that HPA ring closure is first-order in HPA concentration, and regression of each data set yields an apparent rate constant into which the concentration of dissociated protons has been lumped (eq 14). Figure 6b plots these apparent rate constants calculated against the measured concentration of solvated protons on a logarithmic scale, and examination of the correlation between k' and C_{H^+} again reveals a first-order dependence. First-order dependencies on HPA and proton concentrations are consistent with prior descriptions of the intramolecular esterification of HPA in homogeneous systems.[74,75]

3.3.2. Temperature Effects. Having established reaction orders for both HPA and H^+, the rate constant, k, can be explicitly determined, and batch kinetic studies were carried out at various temperatures to quantify Arrhenius parameters. Rate constants determined at each temperature are plotted on a logarithmic scale against inverse temperature in Figure 7. Regression of this data indicates that the pre-exponential factor and activation barrier for the intramolecular esterification of HPA are, respectively, 2.0×10^{10} L mol^{-1} s^{-1} and 70 ± 0.4 kJ mol^{-1}. We note that this barrier is slightly higher than that observed for LA hydrogenation (48 kJ mol^{-1}, Section 3.2.2). This result is consistent with our observations that ring closure appears to control GVL production rates at low temperatures and that GVL selectivities improve relative to HPA with increasing reaction temperature.

3.4. Kinetic Model for GVL Production via LA Hydrogenation. With reaction orders and temperature dependencies for both heterogeneously catalyzed LA hydrogenation and homogeneously catalyzed HPA ring closure established, the two reactions can be modeled independently to predict both LA hydrogenation rates and GVL selectivities over Ru/C. The reaction pathway and empirical kinetic parameters

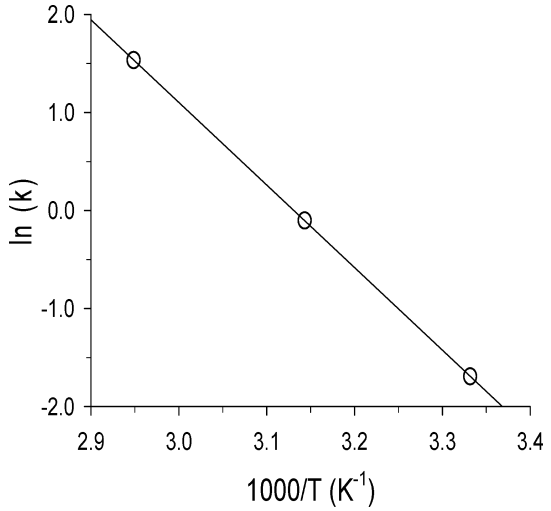

Figure 7. Arrhenius plot illustrating the temperature dependence of rate constants for intramolecular esterification of HPA. Apparent rate constants are reported here in units of L mol^{-1} min^{-1}.

derived from experimental observations summarized to this point are compiled in Scheme 2.

Using these parameters and rate equations, packed bed reactors employed for LA hydrogenation were modeled to reconcile predicted hydrogenation rates and product selectivities with those observed experimentally. The system can be described using the material balances summarized in eqs 15−17.

$$\frac{dF_{LA}}{dV} = -k_1 \cdot \rho_b \cdot c_{H_2}{}^{1/2} \tag{15}$$

$$\frac{dF_{HPA}}{dV} = k_1 \cdot \rho_b \cdot c_{H_2}{}^{1/2} - k_2 \cdot c_{HPA} \cdot c_{H^+} \tag{16}$$

$$\frac{dF_{GVL}}{dV} = k_2 \cdot c_{HPA} \cdot c_{H^+} \tag{17}$$

The catalyst mass in the system is calculated as a product of the system volume and ρ_b, the bulk density of the catalyst bed, and the concentration of solvated protons is calculated on the basis of acid dissociation constants and concentrations of LA

dx.doi.org/10.1021/cs401177p | ACS Catal. 2014, 4, 1171−1181

Scheme 2. Summary of the Empirical Kinetic Model Employed Here To Predict LA Hydrogenation Rates and GVL Selectivities in a Differential Packed Bed Reactor Operating between T = 303 and 343 K, C_{LA} = 0.025−1.5 M, and C_{H_2} = 0.0028−0.028 M

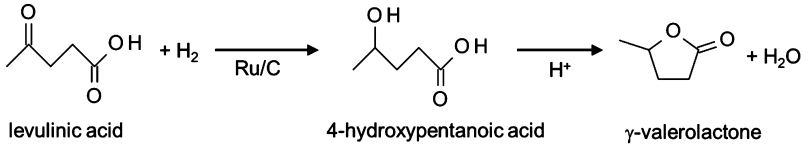

LA Hydrogenation

$$r_1 = A_1 \cdot \exp\left(\frac{-E_{A1}}{R \cdot T}\right) \cdot c_{H_2}^{\frac{1}{2}}$$

HPA Ring Closure

$$r_2 = A_2 \cdot \exp\left(\frac{-E_{A2}}{R \cdot T}\right) \cdot C_{HPA} \cdot C_{H^+}$$

Parameter	Value	Units	Parameter	Value	Units
A_1	6.2 x 10^3	$\frac{(\text{mol L})^{0.5}}{\text{g s}}$	A_2	2.0 x 10^{10}	$\frac{\text{L}}{\text{mol s}}$
E_{A1}	48	kJ mol^{-1}	E_{A2}	70	kJ mol^{-1}

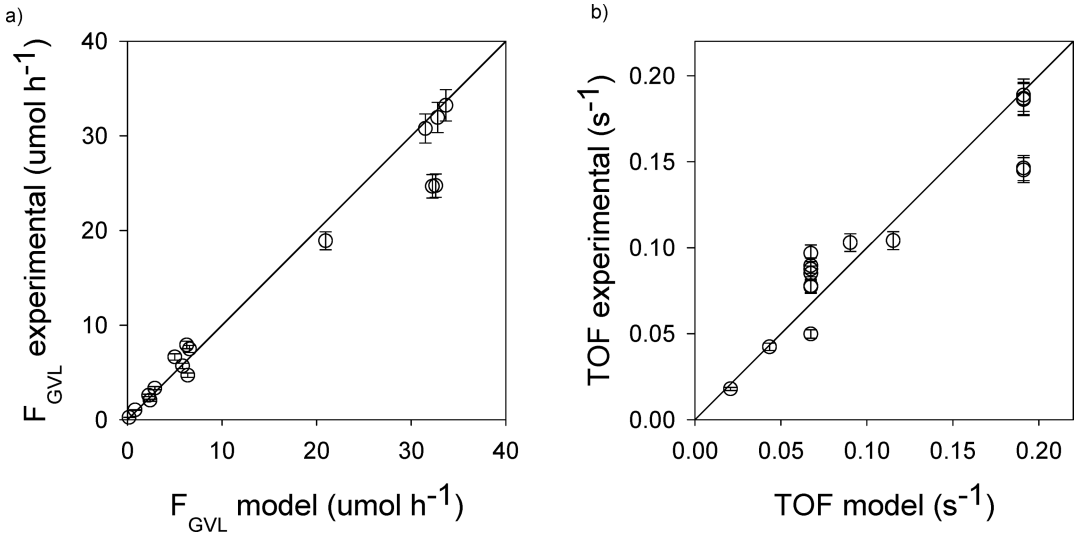

Figure 8. Comparison between model predicted trends and experimental observations at various LA and H_2 concentrations below 363 K. (a) Trends observed in GVL production rates, which captures selectivity during LA hydrogenation. (b)Trends in TOF of LA hydrogenation.

and HPA. As detailed in the Materials and Methods section, carboxylic acid dissociation is expected to vary minimally over the range of temperatures considered here, and its effect was neglected in our calculations. Modeling this system is complicated slightly by the fact that LA hydrogenation is heterogeneously catalyzed on Ru sites, and HPA ring closure is homogeneous. Thus, LA hydrogenation occurs only in the relatively small Ru/C bed, whereas HPA ring closure occurs homogeneously throughout both the Ru/C bed and in reactor sections filled with inert packing. To address this issue, reactors were simulated as being composed of separate hydrogenation and inert sections, and the effluent from the hydrogenation section was used as the input to the inert section. As illustrated in Figure 8, we were able to reconcile, without further adjustment of parameters, predicted LA hydrogenation turnover frequencies and GVL production rates in each of the differential kinetic studies summarized in sections 3.2.1 and 3.2.2, indicating that the empirical model developed here is sufficient for predicting both LA conversion and GVL selectivity in kinetically controlled regimes. Since the catalysts employed here are deactivating, the steady state balances given by eqs 15−17 apply only for prediction of initial LA hydrogenation and GVL production rates, and the data summarized in Figure 8 indicate values estimated at zero time on-stream. On the basis of replicates of rate data collected at a well-defined reference condition (C_{LA} = 0.5 M, C_{H_2} = 0.016 M, T = 323 K), rates of LA hydrogenation and GVL production measured in this system deviate by roughly 5% from the mean, and the error bars in Figure 8 reflect this uncertainty.

3.5. Stacked Bed Reactors. Results from the preceding sections indicate that LA hydrogenation turnover frequencies are reasonable at near ambient temperatures (e.g., ∼0.08 s^{-1} at 323 K, 0.5 M LA, 0.016 M H_2) and that transport limitations become significant as temperatures increase substantially beyond this point. At low temperatures, we additionally observe that HPA ring closure appears to control the rate of GVL production such that GVL selectivity is <5%, independent of LA conversion. Increasing reaction temperature improves GVL selectivity because ring closure has a slightly larger activation barrier (70 kJ mol^{-1}) than LA hydrogenation (48 kJ

dx.doi.org/10.1021/cs401177p | ACS Catal. 2014, 4, 1171−1181

mol^{-1}), and we observe nearly 80% selectivity to GVL during differential LA hydrogenation at 423 K. However, high temperature operation is perhaps an inefficient choice for increasing productivity over a 5 wt % Ru/C catalyst. Pore diffusion quickly becomes rate controlling such that dramatic increases in reaction temperature yield only marginal enhancement in hydrogenation rates (e.g., 0.08 s^{-1} at 323 K compared with 0.6 s^{-1} at 423 K); thus, the additional investment in energy input is not fully recovered as substantially decreased residence times for LA hydrogenation. Results summarized thus far demonstrate that the rate of HPA esterification scales with proton concentration. Therefore, an alternate approach to improving GVL selectivity is to introduce a second, acidic catalyst to expedite ring closure. Although many homogeneous and heterogeneous combinations of Ru and acidity are likely possible, we have employed a simple, stacked bed of Ru/C followed by A15 to facilitate sequential hydrogenation of LA and intramolecular esterification of HPA. Although the same outcome could be more elegantly accomplished using a bifunctional catalyst, introducing acidity in parallel to hydrogenation may encourage angelicalactone formation and, thus, alter the kinetics of GVL formation according to Scheme 1. By separating metal and acid functionalities, we were able to directly probe the hypothesis that expediting HPA ring closure improves GVL production rates without altering LA hydrogenation rates. Observed stacked-bed hydrogenation rates and product selectivities are summarized in Table 2.

Table 2. Experimentally Observed LA Conversions and Product Selectivities during Hydrogenation of LA over Ru/C and A15[a]

					STY (s^{-1})		selectivity (%)	
run	WHSV[b] (h^{-1})	WHSV[c] (h^{-1})	X_{LA} (%)	TOF (s^{-1})	HPA	GVL	HPA	GVL
1	550	0	2	0.107	0.104	0.003	97	3
2	560	16.8	2	0.093	0.074	0.019	80	20
3	5	0	99		0.056	0.003	95	5
4	5	0.15	92		0.007	0.048	12	88

[a] T = 323 K, C_{LA} = 0.5 M (Entries 1 and 2), 0.1 M (Entries 3 and 4), C_{H_2} = 0.016 M. [b] LA weight hourly space velocity based on Ru/C loadings. [c] LA weight hourly space velocity based on Amberlyst-15 loadings.

Control experiments carried out under differential conditions (entries 1 and 2) illustrate that, despite employing different Ru/C pretreatment protocols (i.e., in situ vs ex situ reduction), hydrogenation rates over Ru/C are not altered in the stacked bed reactor. Entry 2 shows that even a small quantity of A15 resin drastically shifts product selectivity toward GVL; however, conversions (<2%) and selectivities (<20%) remain below what would be desirable in a practical implementation. Entry 3 demonstrates that complete conversion of LA via hydrogenation over Ru/C at 323 K is achieved at a weight hourly space velocity of 5 h^{-1}; however, GVL selectivity remains poor over the metal catalyst. By adding a second bed of A15 (entry 4), product selectivity can be shifted almost entirely to GVL at 323 K, facilitating nearly 80% yield of GVL at practical residence times in a single reactor.

CONCLUSION

We have shown that LA can be hydrogenated at near ambient temperatures, proceeding primarily through a HPA-mediated pathway in which hydrogenation occurs first and is followed by acid-catalyzed dehydration. At low temperatures, intramolecular esterification of HPA appears to control the rate of GVL formation, whereas at high temperatures, mass transfer limits the rate of hydrogenation. By recognizing this and developing an understanding of the kinetics of the sequential hydrogenation and dehydration steps, we have demonstrated that it is possible to leverage a strongly acidic catalyst in conjunction with a hydrogenation metal to significantly improve GVL production rates at low temperatures. With respect to rational design, it appears that LA hydrogenation is best-suited to bifunctional catalysts exhibiting hydrogenation functionality alongside acidity. We have additionally observed pronounced deactivation of monometallic Ru/C in this model system, even under mild conditions. Although underlying causes have not been conclusively established, sintering appears to cause an irreversible loss of activity, suggesting that it is critical to identify strategies for retaining metal dispersion during aqueous phase hydrogenation.

ASSOCIATED CONTENT

Supporting Information

Consideration of interphase transport of H_2 to allow calculation of dissolved H_2 concentrations; consideration of interparticle heat and mass transfer on LA hydrogenation rates; consideration of intraparticle heat and mass transfer on LA hydrogenation rates; operational limits for kinetic control in LA hydrogenation; analytical procedures for quantification of LA, GVL, and HPA in reactor samples. This information is available free of charge via the Internet at http://pubs.acs.org/.

AUTHOR INFORMATION

Corresponding Author

*Address: Department of Biomedical and Chemical Engineering, 329 Link Hall, Syracuse University, Syracuse, NY 13244. Phone: 315-443-2550. E-mail: jqbond@syr.edu.

Notes

The authors declare no competing financial interest.

ACKNOWLEDGMENTS

The authors acknowledge financial support for this work from the National Science Foundation (CBET, Award No. 1159739). We also thank William P. Dossert and Richard W. Chave (Syracuse University College of Engineering) for their invaluable support in the design and manufacture of laboratory equipment.

REFERENCES

(1) Horvath, I. T.; Mehdi, H.; Fabos, V.; Boda, L.; Mika, L. T. *Green Chem.* **2008**, *10*, 238−242.
(2) Mehdi, H.; Fabos, V.; Tuba, R.; Bodor, A.; Mika, L. T.; Horvath, I. T. *Top. Catal.* **2008**, *48*, 49−54.
(3) Lange, J. P.; Price, R.; Ayoub, P.; Louis, J.; Petrus, L.; Clarke, L.; Gosselink, H. *Angew. Chem. Int. Ed.* **2010**, *49*, 4479−4483.
(4) Bond, J. Q.; Martin Alonso, D.; Wang, D.; West, R. M.; Dumesic, J. A. *Science* **2010**, *327*, 1110−1114.
(5) Bond, J. Q.; Martin Alonso, D.; West, R. M.; Dumesic, J. A. *Langmuir* **2010**, *26*, 16291−16298.
(6) Bond, J. Q.; Wang, D.; Martin Alonso, D.; Dumesic, J. A. *J. Catal.* **2011**, *281*, 290−299.

(7) Serrano-Ruiz, J. C.; Braden, D. J.; West, R. M.; Dumesic, J. A. *Appl. Catal., B* **2010**, *100*, 184−189.
(8) Martin Alonso, D.; Bond, J. Q.; Dumesic, J. A. *Green Chem.* **2010**, *12*, 1493−1513.
(9) Martin Alonso, D.; Bond, J. Q.; Serrano-Ruiz, J. C.; Dumesic, J. A. *Green Chem.* **2010**, *12*, 992−999.
(10) Martin Alonso, D.; Bond, J. Q.; Wang, D.; Dumesic, J. A. *Top. Catal.* **2011**, *54*, 447−457.
(11) Horvath, I. T. *Green Chem.* **2008**, *10*, 1024−1028.
(12) Wettstein, S. G.; Martin Alonso, D.; Chong, Y. X.; Dumesic, J. A. *Energy Environ. Sci.* **2012**, *5*, 8199−8203.
(13) Martin Alonso, D.; Gallo, J. M. R.; Mellmer, M. A.; Wettstein, S. G.; Dumesic, J. A. *Catal. Sci. Technol.* **2013**, *3*, 927−931.
(14) Gurbuz, E. I.; Gallo, J. M. R.; Martin Alonso, D.; Wettstein, S. G.; Lim, W. Y.; Dumesic, J. A. *Angew. Chem., Int. Ed.* **2013**, *52*, 1270−1274.
(15) Martin Alonso, D.; Wettstein, S. G.; Dumesic, J. A. *Green Chem.* **2013**, *15*, 584−595.
(16) Martin Alonso, D.; Wettstein, S. G.; Mellmer, M. A.; Gurbuz, E. I.; Dumesic, J. A. *Energy Environ. Sci.* **2013**, *6*, 76−80.
(17) Luterbacher, J. S.; Rand, J. M.; Martin Alonso, D.; Han, J.; Youngquist, J. T.; Maravelias, C. T.; Pfleger, B. F.; Dumesic, J. A. *Science* **2014**, *343*, 277−280.
(18) Lange, J. P.; Vestering, J. Z.; Haan, R. J. *Chem. Commun.* **2007**, 3488−3490.
(19) Manzer, L. E. *Appl. Catal., A* **2004**, *272*, 249−256.
(20) Wright, W. R. H.; Palkovits, R. *ChemSusChem* **2012**, *5*, 1657−1667.
(21) Lange, J. P.; van de Graaf, W. D.; Haan, R. J. *ChemSusChem* **2009**, *2*, 437−441.
(22) Gurbuz, E. I.; Wettstein, S. G.; Dumesic, J. A. *ChemSusChem* **2012**, *5*, 383−387.
(23) Maldonado, G. M. G.; Assary, R. S.; Dumesic, J. A.; Curtiss, L. A. *Energy Environ. Sci.* **2012**, *5*, 8990−8997.
(24) Gallezot, P. *Chem. Soc. Rev.* **2012**, *41*, 1538−1558.
(25) Van de Vyver, S.; Thomas, J.; Geboers, J.; Keyzer, S.; Smet, M.; Dehaen, W.; Jacobs, P. A.; Sels, B. F. *Energy Environ. Sci.* **2011**, *4*, 3601−3610.
(26) Fitzpatrick, S. W. World Intellectual Property Organization, Patent No. 96/40609 1996.
(27) Fitzpatrick, S. W.; United States Patent Office, Patent No. 5608105 1997.
(28) Bozell, J. J.; Moens, L.; Elliott, D. C.; Wang, Y.; Neuenscwander, G. G.; Fitzpatrick, S. W.; Bilski, R. J.; Jarnefeld, J. L. *Resour., Conserv. Recycl.* **2000**, *28*, 227−239.
(29) Girisuta, B.; Janssen, L. P. B. M.; Heeres, H. J. *Ind. Eng. Chem. Res.* **2007**, *46*, 1696−1708.
(30) Mascal, M.; Nikitin, E. B. *Green Chem.* **2009**, *12*, 370−373.
(31) Heeres, H.; Handana, R.; Chunai, D.; Rasrendra, C. B.; Girisuta, B.; Heeres, H. J. *Green Chem.* **2009**, *11*, 1247−1255.
(32) Deng, L.; Li, J.; Lai, D. M.; Fu, Y.; Guo, Q. X. *Angew. Chem., Int. Ed.* **2009**, *48*, 6529−6532.
(33) Chia, M.; Dumesic, J. A. *Chem. Commun.* **2011**, *47*, 12233−12235.
(34) Yan, K.; Liao, J. Y.; Wu, X.; Xie, X. M. *RSC Adv.* **2013**, *3*, 3853−3856.
(35) Hengne, A. M.; Rode, C. V. *Green Chem.* **2012**, *14*, 1064−1072.
(36) Luo, W. H.; Deka, U.; Beale, A. M.; van Eck, E. R. H.; Bruijnincx, P. C. A.; Weckhuysen, B. M. *J. Catal.* **2013**, *301*, 175−186.
(37) Wu, Z. J.; Ge, S. H.; Ren, C. X.; Zhang, M. H.; Yip, A.; Xu, C. M. *Green Chem.* **2012**, *14*, 3336−3343.
(38) Deng, L.; Zhao, Y.; Li, J. A.; Fu, Y.; Liao, B.; Guo, Q. X. *ChemSusChem* **2010**, *3*, 1172−1175.
(39) Luque, R.; Clark, J. H. *Catal. Commun.* **2010**, *11*, 928−931.
(40) Du, X. L.; Liu, Y. M.; Wang, J. Q.; Cao, Y.; Fan, K. N. *Chin. J. Catal.* **2013**, *34*, 993−1001.
(41) Sen, S. M.; Henao, C. A.; Braden, D. J.; Dumesic, J. A.; Maravelias, C. T. *Chem. Eng. Sci.* **2012**, *67*, 57−67.
(42) Braden, D. J.; Henao, C. A.; Heltzel, J.; Maravelias, C. C.; Dumesic, J. A. *Green Chem.* **2011**, *13*, 1755−1765.
(43) Martin Alonso, D.; Wettstein, S. G.; Bond, J. Q.; Root, T. W.; Dumesic, J. A. *ChemSusChem* **2011**, *4*, 1078−1081.
(44) Wettstein, S. G.; Bond, J. Q.; Martin Alonso, D.; Pham, H. N.; Datye, A. K.; Dumesic, J. A. *Appl. Catal., B* **2012**, *117*−*118*, 321−329.
(45) Sen, S. M.; Gurbuz, E. I.; Wettstein, S. G.; Martin Alonso, D.; Dumesic, J. A.; Maravelias, C. T. *Green Chem.* **2012**, *14*, 3289−3294.
(46) Al-Shaal, M. G.; Wright, W. R. H.; Palkovits, R. *Green Chem.* **2012**, *14*, 1260−1263.
(47) Upare, P. P.; Lee, J. M.; Hwang, D. W.; Halligudi, S. B.; Hwang, Y. K.; Chang, J. S. *J. Ind. Eng. Chem.* **2011**, *17*, 287−292.
(48) Akpa, B. S.; D'Agostino, C.; Gladden, L. F.; Hindle, K.; Manyar, H.; McGregor, J.; Li, R.; Neurock, M.; Sinha, N.; Stitt, E. H.; Weber, D.; Zeitler, J. A.; Rooney, D. W. *J. Catal.* **2012**, *289*, 30−41.
(49) Wan, H.; Raghunath, A. V.; Chaudhari, V.; Subramaniam, B. *J. Catal.* **2014**, *309*, 174−184.
(50) Luo, W.; Deka, U.; Beale, A. M.; van Eck, E. R. H.; Bruijnincx, P. C. A.; Weckhuysen, B. M. *J. Catal.* **2013**, *301*, 175−186.
(51) Walde, A. W. *J. Phys. Chem.* **1939**, *43*, 431−438.
(52) Martin, A. W.; Tartar, H. V. *J. Am. Chem. Soc.* **1937**, *59*, 2672−2675.
(53) Harned, H. S.; Ehlers, R. W. *J. Am. Chem. Soc.* **1933**, *55*, 2379−2383.
(54) Reijenga, J. C.; Gagliardi, L. G.; Kenndler, E. *J. Chromatogr., A* **2007**, *1155*, 142−145.
(55) Washburn, E. W. In *International Critical Tables of Numerical Data, Physics, Chemistry and Technology*; McGraw-Hill: New York, 1930; Vol. 7, p 140.
(56) Pérez-Prior, M. T.; Manso, J. A.; del Pilar García-Santos, M.; Calle, E.; Casado, J. *J. Org. Chem.* **2004**, *70*, 420−426.
(57) Bartholomew, C. H. *Appl. Catal., A* **2001**, *212*, 17−60.
(58) Besson, M.; Gallezot, P. *Catal. Today* **2003**, *81*, 547−559.
(59) Maris, E. P.; Ketchie, W. C.; Oleshko, V.; Davis, R. J. *J. Phys. Chem. B* **2006**, *110*, 7869−7876.
(60) Schuurman, Y.; Kuster, B. F. M.; van der Wiele, K.; Marin, G. B. *Appl. Catal., A* **1992**, *89*, 47−68.
(61) Crezee, E.; Hoffer, B. W.; Berger, R. J.; Makkee, M.; Kapteijn, F.; Moulijn, J. A. *Appl. Catal., A* **2003**, *251*, 1−17.
(62) Fabre, L.; Gallezot, P.; Perrard, A. *J. Catal.* **2002**, *208*, 247−254.
(63) Singh, U. K.; Vannice, M. A. *AIChE J.* **1999**, *45*, 1059−1071.
(64) Singh, U. K.; Vannice, M. A. *J. Catal.* **2000**, *191*, 165−180.
(65) Cortright, R. D.; Goddard, S. A.; Rekoske, J. E.; Dumesic, J. A. *J. Catal.* **1991**, *127*, 342−353.
(66) Boudart, M.; Djéga-Mariadassou, G. *Kinetics of Heterogeneous Catalytic Reactions*; Princeton University Press: Princeton, NJ, 1984.
(67) Rachmady, W.; Vannice, M. A. *J. Catal.* **2000**, *192*, 322−334.
(68) Vaidya, P. D.; Mahajani, V. V. *Chem. Eng. Sci.* **2005**, *60*, 1881−1887.
(69) Tike, M. A.; Mahajani, V. V. *Can. J. Chem. Eng.* **2006**, *84*, 452−458.
(70) Neri, G.; Bonaccorsi, L.; Galvagno, S. *Ind. Eng. Chem. Res.* **1997**, *36*, 3554−3562.
(71) Jyrki, K.; Mikkola, J. P.; Sparv, M.; Warna, J.; Karhu, H.; Salmi, T. *Chem. Eng. J* **2008**, *139*, 69−77.
(72) Horiuti, I.; Polanyi, M. *Trans. Faraday Soc.* **1934**, *30*, 1164−1172.
(73) Sinha, N. K.; Neurock, M. *J. Catal.* **2012**, *295*, 31−44.
(74) Taylor, H. S.; Close, H. W. *J. Phys. Chem.* **1924**, *29*, 1085−1098.
(75) Fishbein, W. N.; Bessman, S. P. *J. Biol. Chem.* **1966**, *241*, 4842−4847.